

Nuclear equation of state at high density and the properties of neutron stars

P. K. Sahu

Division of Physics, Graduate School of Science
Hokkaido University, Sapporo 060-0810
JAPAN
(February 25, 2019)

Abstract

We discuss the relativistic nuclear equation of state (EOS) using a relativistic transport model in heavy-ion collisions. From the baryon flow for $Au + Au$ systems at SIS to AGS energies and above we find that the strength of the vector potential has to be reduced moderately at high density or at high relative momenta to describe the flow data at 1-10 A GeV. We use the same dynamical model to calculate the nuclear EOS and then employ this to calculate the gross structure of the neutron star considering the core to be composed of neutrons with an admixture of protons, electrons, muons, sigmas and lambdas at zero temperature. We then discuss these gross properties of neutron stars such as maximum mass and radius in contrast to the observational values.

PACS number(s): 26.60.+c, 21.65.+f

I. INTRODUCTION

The nuclear equation of state (EOS) at high density is still an unresolved issue though many theoretical and experimental efforts have been made in the last two decades to address this question in a more systematic way. Theoretically, specially in astrophysics, the density of the core inside the compact objects like neutron star is greater than normal nuclear matter density, composed of many non-strange and strange degrees of freedom. One of the most important characteristic feature of a neutron star is its maximum allowed mass. The determination of maximum mass and radius of neutron star are dominated by the interactions between particles at high density and its EOS. There are many models available in the literature to deal with maximum masses of neutron stars. These are relativistic and non- relativistic approaches. The non- relativistic models [1,2] based on the potential approach describe the nuclear structure for light nuclei. However, the relativistic models [3–7] constructed from Lagrangian approach explain the nuclear structure data for heavy nuclei without violating the properties of nuclear matter at saturation density. In both conventional approaches in the neutron star matter, the estimated maximum masses of neutron star are above $2M_{\odot}$. Recently from several calculations, it has been pointed out [8–10] that the nuclear EOS should be soft at high density. This is due to fact that all the measured neutron star masses are less than $2M_{\odot}$ [11]. Various scenarios including the reduced strength of vector field, the presence of hyperons and possibility of kaon condensation, have been proposed to be soften the EOS.

Regarding the composition of neutron star matter, there are calculations [12], which include kaons as the strange particles along with neutrons and protons e.g., the possibility of kaon condensation. Also there are models [5,6] in the neutron star matter where the composition of particles are sigmas and lambdas as strange particles besides neutrons, protons and electrons as non- strange particles. Both these proposed models in the neutron star matter lead to a soft EOS at high density. In this paper we consider the existence of hyperons in the neutron star matter with the recent compiled information of nuclear interaction from heavy-ion collisions.

Experimentally, the nuclear EOS is very important to understand the non- equilibrium complicated heavy- ion collisions data at very high energies. Very recently [13,14], the heavy- ion collisions data such as the sideward and elliptic flow have been measured at AGS energies. The sideward flow data are mainly determined by the nature of the nuclear force in the nuclear EOS. Moreover, the nuclear EOS can be understood better from the elliptic flow than sideward flow, because the elliptical flow plays less uncertainties role in the opposing stream of matter moving past each other within the reaction plane in the heavy-ion collisions. Recently, the beam energy dependence of flow data [13,14] indicate that the nuclear EOS is rather soft to lead a possible phase transition to quark gluon plasma at high density and hence the strength of the repulsive vector potential must be low to describe these data in the heavy- ion collisions.

In the present discussion, we use an extended version of relativistic mean field model [15] including the momenta dependent forces, which are taken into account phenomenologically in the relativistic transport model in heavy- ion collisions. We calculate the nuclear EOS by using the same dynamic momentum dependence constraints in the nuclear potentials and then employ to the neutron star structure calculations. The aim of this paper is to derive

the nuclear force from the heavy-ion collisions data e.g., from nucleon flow data and then to study this force on the gross structure of the neutron star by giving less importance to the composition of neutron star matter. As far as the strange particles are concerned, we take minimum strange particles (Σ and Λ) in the neutron star matter calculation at high densities.

The paper is organized as follows: In section 2 we briefly describe the relativistic nuclear EOS and its derivation from heavy- ion reactions. In section 3 we employ the same nuclear EOS to the neutron star structure with the systematic results. The conclusion and summary are presented in section 4.

II. RELATIVISTIC NUCLEAR EQUATION OF STATE

The relativistic mean- field theory is very successful model in the relativistic transport model in heavy- ion collisions as well as in nuclear structure physics. Originally, Walecka [3] had proposed the relativistic mean- field model and later the modified version of this has been used widely to calculate nuclear structure and nuclear matter properties. The extended version of the Walecka model, so called non- linear relativistic mean- field model [4,6] has the interaction of Dirac nucleons with scalar and vector mesons as well as non- linear self- interaction of the scalar field. The extra non- linear self- interaction scalar field helps to get the empirical values of bulk properties of nuclear matter at saturation density, e.g., the nuclear incompressibility and the value of effective nucleon mass in the desirable range. The physics behind this phenomenological successful model is that the nucleon- nucleon interaction in the mean- field theory contains strong attractive Lorentz scalar and repulsive Lorentz vector components, which almost cancel for low momenta, but produce a strong spin- orbit force consistent with the observed single- particle spectra. In the original Walecka model [3], the vector potential increases linearly with density, whereas the scalar potential changes non- linearly. This is because the vector and scalar potentials have linear and non- linear function of density respectively. However, from the heavy- ion collisions data, we find that the vector potential also should have non- linear function of baryon density, i.e., the strength of the vector potential should be low at high density [15] compared to the original model [3]. Recently, this fact has been taken by adding the non- linear vector meson terms in the original Lagrangian density and applied to the nuclear matter, neutron star matter [10] and nuclear structure [16] calculations. In our calculation, we take the non- linear effect in the vector meson with density by employing the phenomenological momentum dependent cut- off to the vector potential term. We adopt this method keeping in mind to describe the heavy- ion reactions data at high energies, which generates the nuclear matter like situation in the laboratory. We recall that the mean-field energy density for nuclear matter in the relativistic mean-field model can be written as [4]

$$\begin{aligned} \varepsilon(m^*, n_b) = & g_v V_0 n_b - \frac{1}{2} m_v^2 V_0^2 + \frac{m_s^2}{2g_s^2} (m - m^*)^2 + \frac{B}{3g_s^3} (m - m^*)^3 \\ & + \frac{C}{4g_s^4} (m - m^*)^4 + \gamma \int_0^{k_f} \frac{d^3 p}{(2\pi)^3} \sqrt{(p^2 + m^*)}, \end{aligned} \quad (1)$$

where $m^* = m - g_s S_0$ is the effective nucleon mass, n_b is the baryon density and the spin and isospin degeneracy is $\gamma = 4$. S_0 and V_0 are the scalar and vector fields with mass m_s

and m_v , which couple to nucleons with coupling constants g_s and g_v , respectively. B and C are constant parameters describing the scalar self-interactions field and p is the nucleon momentum integrated up to the Fermi momentum k_f . In (1), the vector and scalar potentials depend on density, however, the vector potential increases linearly with density (n_B). The parameters g_v , g_s , B and C in (1) are determined by fitting the saturation density, binding energy, effective nucleon mass and the compression modulus at nuclear matter density (cf. NL3 parameters set from Table I in Ref. [4]).

In our present calculation, we have extended (1) to include a non-linear dependence of the vector potential on the baryon density by implementing the momentum (p) dependent form factor at the vertices and can be written as [15]

$$V_0(p) = V_0 \frac{p^2 - \Lambda_{v1}^2}{p^2 + \Lambda_{v2}^2}, \quad (2)$$

where the cut- off parameters $\Lambda_{v1} = 0.37$ GeV, $\Lambda_{v2} = 0.9$ GeV and V_0 is vector potential. For completeness, we incorporate the momentum dependent form factor at the scalar vertices in the form given as [15]

$$V_s(p) = V_s \frac{p^2 - \Lambda_{s1}^2}{p^2 + \Lambda_{s2}^2}, \quad (3)$$

where the cut- off parameters $\Lambda_{s1} = 0.71$ GeV, $\Lambda_{s2} = 1.0$ GeV and V_s is scalar potential. The choice of these form factors are similar to that used in effective meson-exchange interactions for nucleon-nucleon scattering [17] and later this strategy was used in relativistic approach for nucleus-nucleus collisions from SIS to SPS energies [18]. The values of cut-off parameters in vector and scalar vertices are chosen to describe properly the Schrödinger-equivalent potential until 1 GeV and the flow data at AGS energies. These cut-off parameters are not unique for various type of equation of states to fit Schrödinger-equivalent potential until 1 GeV and the flow data at AGS energies simultaneously. We note that the form factor eq.(2) will make the vector interaction weak at high baryon density and at high energies in heavy-ion collisions. At these energies, it has also been observed that the strength of repulsive vector potential should be reduced considerably at high density or at high relative momenta to describe the flow data. Theoretically, it is important to understand the decrease of vector coupling at high density. Contrast to heavy-ion reactions, in this line some works have been performed [19] and more to be required in details [20].

We show in Fig. 1, the scalar and vector potential energies as a function of baryon density. The solid lines (NLE curves) are associated with the momentum dependent form factors given in eqs(2,3) that describe the flow data best from SIS to AGS energies. The dashed lines (NL3 curves) are without momentum dependent potentials. The vector part for NLE is substantially low at high baryon density as that of NL3 parameter set. At high density the reduction of vector potential is more significant than the scalar potential for NLE curves. Therefore, the net effect of changed potentials is vector potential due to substantial reduction of vector part at high baryon density. For example, at $\rho = 8\rho_0$, the values of vector part and scalar part are 1250 MeV and -511 MeV respectively for NLE, where the value of vector part is 1740 MeV and scalar part is -735 MeV for NL3. So, the net reduction is dominated by the vector potential in NLE model. The corresponding EOS versus baryon density are shown in Fig. 2 for extended momentum dependent model (NLE) as well as the

original non- linear model (NL3). NLE has the momentum dependent form factor in the vector and scalar potentials. The other nuclear EOS has been discussed more details in the Ref. [6] by varying the nuclear incompressibility from low (soft) 250 MeV to high (stiff) 350 MeV values. We do not elaborate on that issue here, because we would like to emphasize more on the momentum dependent force in the nuclear EOS along the line of heavy-ion reaction data. We see in Fig. 2 that NLE nuclear EOS is softer than NL3 at density $\geq 7\rho_0$ and is slightly stiffer at density $\leq 7\rho_0$. The incompressibility is close (~ 380 MeV) to NL3 value at saturation density. In the next section, we would like to implement this model in the neutron star matter, where the core density is in the range of $> 5 - 8\rho_0$. So, in the present model, the stiffness of equation of state changes around that density, due to the main contribution coming from the reduced vector potential. However, in the heavy- ion flow calculation at AGS energies, the stiffness of equation of state not only comes from the net reduction of vector potential but also from the transition from hadron to string degrees of freedom as discussed in our recent work [15]. It has been pointed out recently [21] from the simulation calculation that one might even reach $10\rho_0$, although only for a very short time of a few fm/c at energy range between the AGS and the SPS energies. Hence at AGS energy range, the baryon density is expected to reach more than $> 5\rho_0$.

Recently, the elliptic flow and the sideward flow have been studied theoretically with increasing beam energy by various type of equation of state and the possible signature of phase transition [22]. More precisely, the beam energy dependence of the observed elliptic flow has been interpreted such a possible phase transition. The reason is that a simulation model including different kinds of equation of state is consistent with a softening of the equation of state. This softening of equation of state can be realized in many ways, for example: (i) by reducing the strong repulsive force in the equation of state with help of momentum dependent form factor and fitting it with Schrödinger-equivalent potential and (ii) by implementing transition from hadronic to string degrees of freedom with beam energies in the simulation model [15]. In our calculation, we implement the former one, where the thermodynamic pressure in the extended model NLE is lower as compared to the NL3 model due to less repulsive force at AGS energy regime. We thus get reduced repulsive force because of the strong cut-off parameters eq. (2) in the vector potential. Also this cut-off makes the vector potential non-linear function of baryon density.

III. NEUTRON STAR MATTER AND PROPERTIES OF NEUTRON STAR

A. Neutron star matter

The core of the neutron star plays a significant role to determine the gross structural properties like maximum mass and radius of the neutron star. The density of the core inside the neutron star is greater than the normal nuclear matter density and hence the nuclear interactions are important to construct the neutron star matter EOS around that density. Moreover, in such a high density, the strange particles are expected to be present along with usual neutron matters like neutrons, protons and electrons. So, in our neutron star matter calculation we assume that the core of the neutron star matter is composed of neutrons with an admixture of protons, electrons, muons and hyperons (Λ and Σ^-) [6]. The concentrations

of each particle can be determined by using the condition of equilibrium under the weak interactions (assuming that neutrinos are not degenerate) and the electric charge neutrality:

$$\begin{aligned}\mu_p &= \mu_n - \mu_e, \quad \mu_\Lambda = \mu_n, \\ \mu_{\Sigma^-} &= \mu_n + \mu_e, \quad \mu_\mu = \mu_e; \\ n_p &= n_e + n_\mu + n_{\Sigma^-}.\end{aligned}\tag{4}$$

In addition, the total baryon density is $n_B = n_n + n_p + n_\Lambda + n_{\Sigma^-}$ and the baryon chemical potential is $\mu_B = \mu_n$, where n_i and μ_i stand for number density and chemical potential for i -th particle respectively.

Since the nuclear force is known to favor isospin symmetry and the symmetry energy arising solely from the Fermi energy is known to be inadequate to account for the empirical value of the symmetry energy (~ 32 MeV), we include the interaction due to isospin triplet ρ - meson in the relativistic non- linear mean field model for the purpose of describing the neutron- rich matter [7]. It is noted that the ρ - meson will contribute a term $= \frac{g_\rho^2}{8m_\rho^2}(n_p - n_n)^2$ to the energy density and pressure. We fix the coupling constant g_ρ by requiring that the symmetric energy coefficient correspond to the empirical value 32 MeV. Then the neutron star matter EOS is calculated from energy density ε and pressure P are given as follow [6]:

$$\begin{aligned}\varepsilon &= \frac{1}{2}m_v^2V_0^2 + \frac{1}{2}m_\rho^2\rho_0^2 + \frac{1}{2}m_s^2S_0^2 + \frac{B}{3}S_0^3 \\ &\quad + \frac{C}{4}S_0^4 + \sum_i \varepsilon_{FG} + \sum_l \varepsilon_{FG} \\ P &= \frac{1}{2}m_v^2V_0^2 + \frac{1}{2}m_\rho^2\rho_0^2 - \frac{1}{2}m_s^2S_0^2 - \frac{B}{3}S_0^3 \\ &\quad - \frac{C}{4}S_0^4 + \sum_i P_{FG} + \sum_l P_{FG}\end{aligned}\tag{5}$$

where ρ_0 is the third component in isospin space. In the above equations ε_{FG} and P_{FG} are the relativistic non- interacting energy density and pressure of the baryons (i) and leptons (l) respectively.

The three coupling constant parameters of hyperon- meson interaction are not well known. Therefore, we fix the ratio of hyperon-meson and nucleon-meson couplings for σ , ω and ρ mesons respectively (i) by choosing very close to the quark counting rule [6] e.g., the potentials seen by Λ and Σ in nuclear matter are ~ -30 MeV [23] and (ii) assuming the attractive potential seen by Λ and repulsive potential seen by Σ to be ~ -30 MeV [23] and $\sim +10$ MeV [9,24,25] respectively, at nuclear matter density. The analysis of various experimental data on hypernuclei [23–26] suggest that the strength of Σ potential may be either repulsive or attractive at nuclear matter density. This point will be cleared further after analysis of more hypernuclei data in near future and the general discussions are given in recent Ref. [27]. Due to this fact, we consider the two possibility of strength on Σ potential as discussed above.

Taking all these parameters into the equations (4), we show the concentration of particles ($x_i = n_i/n_B$, $i=p, \Sigma$ and Λ) versus baryon density for NLE1, NLE2 and NL3 models in Fig. 3. We display p , Σ and Λ particles in this figure due to practical importance in neutron stars, for example, p fraction plays role for cooling process of neutron stars and the order

of appearance of strange particles with density may influence the EOS of the neutron star matter. In NLE1 and NL3 models, the potentials for Λ and Σ are taken to be equal to ~ -30 MeV, where the potentials for Λ and Σ are chosen to be ~ -30 MeV and $\sim +10$ MeV respectively in NLE2 model. However, the momentum dependent cut-off to the vector potential are incorporated in both NLE1 and NLE2 models. We notice in Fig. 3 that the concentration of particles like Σ^- and Λ start appearing after 2 times nuclear matter density for all models. In NLE1 and NL3 models, the order of appearance of strange particles (first Σ and then Λ) are same due to equal strength of potential felt by strange particles. Where the situation is quite different in case of NLE2 model, here Λ appears first around > 2.5 time nuclear matter density and Σ^- starts coming much later [9] around > 3.5 times nuclear matter density. This is due to fact that Σ sees extra strength $+40$ MeV potential than Λ potential, which is repulsive. In both NLE1 and NLE2 models, the strange particles start coming slightly later than NL3, due to reduction of vector potential by momentum dependent cut-off as given in equation (2). However, the change of proton concentration is not very significant with density for all models, except the slight decreasing tendency at high density was shown by NLE2. At around 1.5 times nuclear matter density, the value of protons concentration crosses the threshold value 0.11 (horizontal line in Fig. 3), which shows that the direct URCA process is possible to lead for cooling of the neutron stars in all models [28].

B. Maximum mass and radius of neutron star

The gross structure of the neutron stars such as mass and radius are calculated from the equations that describe the hydrostatic equilibrium of degenerate stars without rotation in general relativity is called Tolman-Oppenheimer- Volkoff (TOV) equations [7]. From the dynamics and transport properties of pulsars, the additional structure parameters of neutron stars like the moment of inertia I and the surface red shift $z = \frac{1}{\sqrt{1-2GM/Rc^2}} - 1$ are important and are given more elaborately in Ref. [7].

We solve the TOV equations by constructing the EOS for the entire density region starting from the higher density at the center to the surface density. The composite EOS for the entire neutron star density span was constructed by joining the NLE and NL3 neutron star matter EOS to that EOS of the density range (i) 10^{14} to $5 \times 10^{10} \text{ g cm}^{-3}$ [29], (ii) $5 \times 10^{10} \text{ g cm}^{-3}$ to 10^3 g cm^{-3} [30] and (iii) less than 10^3 g cm^{-3} [31]. The composite neutron star matter EOS are plotted in Fig. 4 for NLE1, NLE2 and NL3 models, which are used to calculate the neutron star structures as discussed above. From Fig. 4 we find that the pressure is low at high density for NLE1, NLE2 EOS and hence the soft EOS compare to NL3 EOS. If we look at the Fig. 3, the order of appearance of Λ particles with density reflect in the same order of the nature of EOS. That is, NL3 is stiffer than NLE1 and NLE2 EOS, because the momentum dependent form factor in later two models has reduced the vector potential at high density. So, NLE2 is similar to NLE1 EOS, except a slight stiffer than NLE1 due to the strong repulsive potential present on Σ particles as can be seen in Fig. 4. We also notice in Fig.4 that the NLE2 EOS does not change significantly on the choice of repulsive Σ potential in contrast to NLE1 EOS.

The predicted maximum neutron star masses are very close to the observational values for

NLE1 and NLE2 EOS. The results for the neutron star structure parameters are tabulated in Table I and central density vs mass are plotted in Fig 5. From Fig. 5 and Table I, we observe that the maximum masses of the stable neutron stars are $2.18M_{\odot}$, $1.94M_{\odot}$ and $1.97M_{\odot}$ and corresponding radii are $11.9km$, $10.7km$ and $10.8km$ for NL3, NLE1 and NLE2 EOS respectively. The corresponding central densities are $2.0 \times 10^{15} g cm^{-3}$, $2.2 \times 10^{15} g cm^{-3}$ and $2.2 \times 10^{15} g cm^{-3}$ (> 7 times nuclear matter density) for NL3, NLE1 and NLE2 respectively at the maximum neutron star masses. These maximum masses calculate in our models are in the range of recent observations [32–35], where the observational consequence are discussed below. Very recently, it has been observed that the best determined neutron star masses [11] are found in binary pulsars and are all lie in the range $1.35 \pm 0.04M_{\odot}$ except for the non-relativistic pulsars PSR J1012+5307 of mass $M = (2.1 \pm 0.8)M_{\odot}$ [32]. There are several X-ray binary masses have been measured, the heaviest among them are Vela X-1 with $M = (1.9 \pm 0.2)M_{\odot}$ [33] and Cygnus X-2 with $M = (1.8 \pm 0.4)M_{\odot}$ [34]. From recent discovery of high-frequency brightness oscillations in low-mass X-ray binaries, the large masses of the neutron star in $QPO4U1820 - 30$ ($M = 2.3)M_{\odot}$ [35] is confirmed and this provides a new method to determine the masses and radii of the neutron stars. We also tabulate the moment of inertia and the surface red shift in Table I, which are important for the dynamic and transport properties of pulsars.

At this point, we argue that the softening of EOS may lead to kaon condensation in neutron stars [36] and hence may give a constraint on the best determined maximum mass [11]. However, we feel that from the KaoS data on kaon production, together with kaon flow from heavy-ion reactions [37], it is important to know the momentum dependent K^+ and K^- potentials in dense matter in contrast to the prediction of the chiral perturbation theory. In the present calculation, we don't explore this, but work is in progress [38] by implementing the same momentum forces as given in eqs (2,3).

IV. SUMMARY

We have described the nuclear EOS in the frame work of relativistic mean field theory using a relativistic transport model in the heavy-ion collisions. From the heavy-ion collisions data, more specifically, the baryon flow for $Au + Au$ systems at SIS to AGS energies and above we noticed that the strength of the vector potential has to be reduced substantially at high density and high relative momenta to describe the experimentally observed flow data at 1-10 A GeV. In a different way, the vector potential should be non- linear function of the baryon density. We took this effect by introducing the momentum dependent cut-off into the vector potential in contrast to the heavy-ion collision data. We use the same dynamic treatment in our relativistic mean field model to calculate the nuclear EOS. It is found that the derived nuclear EOS is moderately soft at density $\geq 7\rho_0$ than the original considered nuclear EOS without momentum dependent potentials. This due to the reduction of repulsive nuclear interaction in the nuclear EOS at high density. We then employ the same nuclear EOS to the neutron star structure calculation.

In the neutron star matter, the core of the neutron stars are considered to be composed of neutrons along with an admixture of protons, electrons, muons and hyperons at zero temperature. The resulting maximum mass of stable neutron stars are $2.18M_{\odot}$, $1.94M_{\odot}$ and $1.97M_{\odot}$ for the NL3, NLE1 and NLE2 models, respectively. We observed that the

maximum mass of the neutron star for NLE1 and NLE2 are lower than that for NL3 due to a reduction of the vector field at higher densities. Also, we noticed that the potential felt by Σ particles is not so relevant to neutron star structure calculation. The corresponding neutron star radii are 11.9 km , 10.7 km and 10.8 km for NL3, NLE1 and NLE2, respectively, whereas the corresponding central densities are $2.0 \times 10^{15} \text{ g cm}^{-3}$, $2.2 \times 10^{15} \text{ g cm}^{-3}$ and $2.2 \times 10^{15} \text{ g cm}^{-3}$ respectively for NL3, NLE1 and NLE2 at the maximum neutron star mass. We found that the maximum mass for NLE1 and NLE2 are in the observable region [32–35], $1.4M_{\odot} < M_{max} < 2.2M_{\odot}$ and the corresponding radius is in between $8\text{--}12\text{ km}$.

The author likes to thank W. Cassing and A. Ohnishi for critical reading and W. Cassing, A. Ohnishi and Y. Akaishi for fruitful discussions. PKS likes to acknowledge the support from the Japan Society for the Promotion of Science, Japan. This work is dedicated to Prof. Bhaskar Datta, who passed away on 3rd November 1999.

TABLES

Table I

ε_c ($g\ cm^{-3}$)	R (km)	M/M_\odot	z	I ($g\ cm^2$)
6.0 E14	10.82	1.00	0.17	9.55 E44
8.0 E14	11.46	1.44	0.26	1.61 E45
1.0 E15	11.54	1.66	0.32	1.94 E45
1.5 E15	11.27	1.89	0.41	2.15 E45
2.0 E15	10.89	1.94	0.45	2.08 E45
2.5 E15	10.55	1.94	0.48	1.96 E45
3.0 E15	10.26	1.93	0.50	1.83 E45
4.0 E15	9.83	1.88	0.51	1.62 E45
6.0 E14	10.87	1.03	0.18	9.93 E44
8.0 E14	11.55	1.48	0.27	1.70 E45
1.0 E15	11.63	1.72	0.33	2.05 E45
1.5 E15	11.36	1.92	0.41	2.24 E45
2.0 E15	10.98	1.97	0.46	2.15 E45
2.5 E15	10.96	1.97	0.47	2.02 E45
3.0 E15	10.37	1.95	0.50	1.88 E45
4.0 E15	9.92	1.89	0.51	1.66 E45
6.0 E14	13.20	1.60	0.25	2.31 E45
8.0 E14	13.26	1.89	0.31	2.84 E45
1.0 E15	13.08	2.04	0.36	3.02 E45
1.5 E15	12.43	2.17	0.44	2.96 E45
2.0 E15	11.85	2.18	0.48	2.72 E45
2.5 E15	11.38	2.16	0.51	2.49 E45
3.0 E15	11.00	2.13	0.53	2.28 E45
4.0 E15	10.40	2.05	0.55	1.95 E45

REFERENCES

- [1] A. Akmal, V. R. Pandharipande and D. G. Ravenhall, Phys. Rev. **C58** (1998) 1804.
- [2] R. B. Wiringa, V. Fiks and A. Fabrocini, Phys. Rev. **C38** (1988) 1010.
- [3] B. D. Serot and J. D. Walecka, Adv. Nucl. Phys. **16** (1986) 1;
- [4] A. Lang, B. Blättel, W. Cassing, V. Koch, U. Mosel and K. Weber, Z. Phys. **A340** (1991) 207.
- [5] N. K. Glendenning, F. Weber and S. A. Moszkowski, Phys. Rev. **C45** (1992) 844.
- [6] S. K. Ghosh, S. C. Phatak and P. K. Sahu, Z. Phys. **A352** (1995) 457;
- [7] P. K. Sahu, R. Basu and B. Datta, Astrophys. J. **416** (1993) 267;
- [8] H. Heiselberg and M. Hjorth-Jensen Astrophys. Jour. **525** (1999) L45.
- [9] S. Balberg and A. Gal, Nucl. Phys. **A625** (1997) 435.
- [10] H. Shen, H. Toki, K. Oyamatsu and K. Sumiyoshi, Nucl. Phys. **A637** (1998) 435.
- [11] S. E. Thorsett and D. Chakrabarty, Astrophys. J. **512** (1999) 288.
- [12] G. Brown, C. Lee, M. Rho and V. Thorsson, Nucl. Phys. **A572** (1994) 693; T. Waas, M. Rho and W. Weise, Nucl. Phys. **A617** (1997) 449.
- [13] H. Liu et al., E895 Collaboration, Nucl. Phys. **A 638** (1998) 451c.
- [14] C. Pinkenburg et al., E895 Collaboration, Phys. Rev. Lett. **83** (1999) 1295.
- [15] P.K. Sahu, A. Hombach, W. Cassing, M. Effenberger and U. Mosel, Nucl. Phys. **A 640** (1998) 493; P.K. Sahu, W. Cassing, U. Mosel and A. Ohnishi, nucl-th/9907002, Nucl. Phys. **A 672** (2000) 376.
- [16] Y. Sugahara and H. Toki, Nucl. Phys. **A579** (1994) 557.
- [17] R. Machleidt, K. Holinde and Ch. Elster, Phys. Reports, **149** (1987) 1.
- [18] W. Ehehalt and W. Cassing, Nucl. Phys. **A 602** (1996) 449.
- [19] C. Song, G. E. Brown, D. Min and M. Rho, Phys. Rev. **C 56** (1997) 2244; Y. Kim and H. K. Lee, nucl-th/9905268; Y. Kim, R. Rapp, G. E. Brown and M Rho, nucl-th/9912061.
- [20] P. K. Sahu et al., work is in progress.
- [21] B. Friman et al., nucl-th/9711065; E. L. Bratkovskaya and W. Cassing, Nucl. Phys. **A 619** (1997) 413.
- [22] H. Liu et al, E895 Collaboration, nucl-ex/0005005; J. Stachel, Nucl. Phys. **A 654** (1999) 119.
- [23] R. E. Chrien and C. B. Dover Ann. Rev. Part. Sci. **39** (1989) 227.
- [24] Y. Yamamoto, S. Nishizaki and T. Takatsuka, in preparation.
- [25] J. Dabrowski, Phys. Rev. **C60** (1999), 025205-1.
- [26] T. Harada and Y. Akaishi, Phys. Lett. **B262** (1991), 205.
- [27] T.A. Rijken, V.G.J. Stoks, and Y. Yamamoto, Phys. Rev. **C59** (1999), 21.
- [28] J. Boguta, Phys. Lett. **B 106** (1981) 255; C. J. Pethick, Rev. Mod. Phys. **64** (1992) 1133.
- [29] J. W. Negele and D. Vautherin, Nucl. Phys. **A207** (1973) 298.
- [30] G. Baym, C. J. Pethick and P. G. Sutherland, Astrophys. J. **170** (1971) 299.
- [31] R. P. Feynmann, N. Metropolis and E. Teller, Phys. Rev. **75** (1949) 308.
- [32] J. van Paradijs, (1998), astro-ph/9802177; The many faces of neutron stars, ed. R. Buccieri, J. van Paradijs and M. A. Alpar, in press.
- [33] O. Barziv, in preparation; M. H. van Kerkwijk, J. van Paradijs and E. J. Zuiderwijk, Astron. & Astrophys. **303** (1995) 497 (have larger uncertainties).
- [34] J. A. Orosz and E. Kuulkers, Mon. Not. Roy. Astron. Soc., (1999) in press.

- [35] M. C. Miller, F. K. Lamb and P. Psaltis, *Astrophys. J.*, **508** (1998) 791.
- [36] G. Q. Li, C. -H. Lee and G. E. Brown, *Phys. Rev. Lett.* **79** (1997) 5241.
- [37] M. D. parland et al., *Phys. Rev. Lett.* **75** (1995) 2100; J. Ritman et al., *Z. Phys. A* **352** (1995) 355; G. Agakichiev et al., *Phys. Rev. Lett.* **75** (1995) 1272.
- [38] P. K. Sahu et al., work in progress.

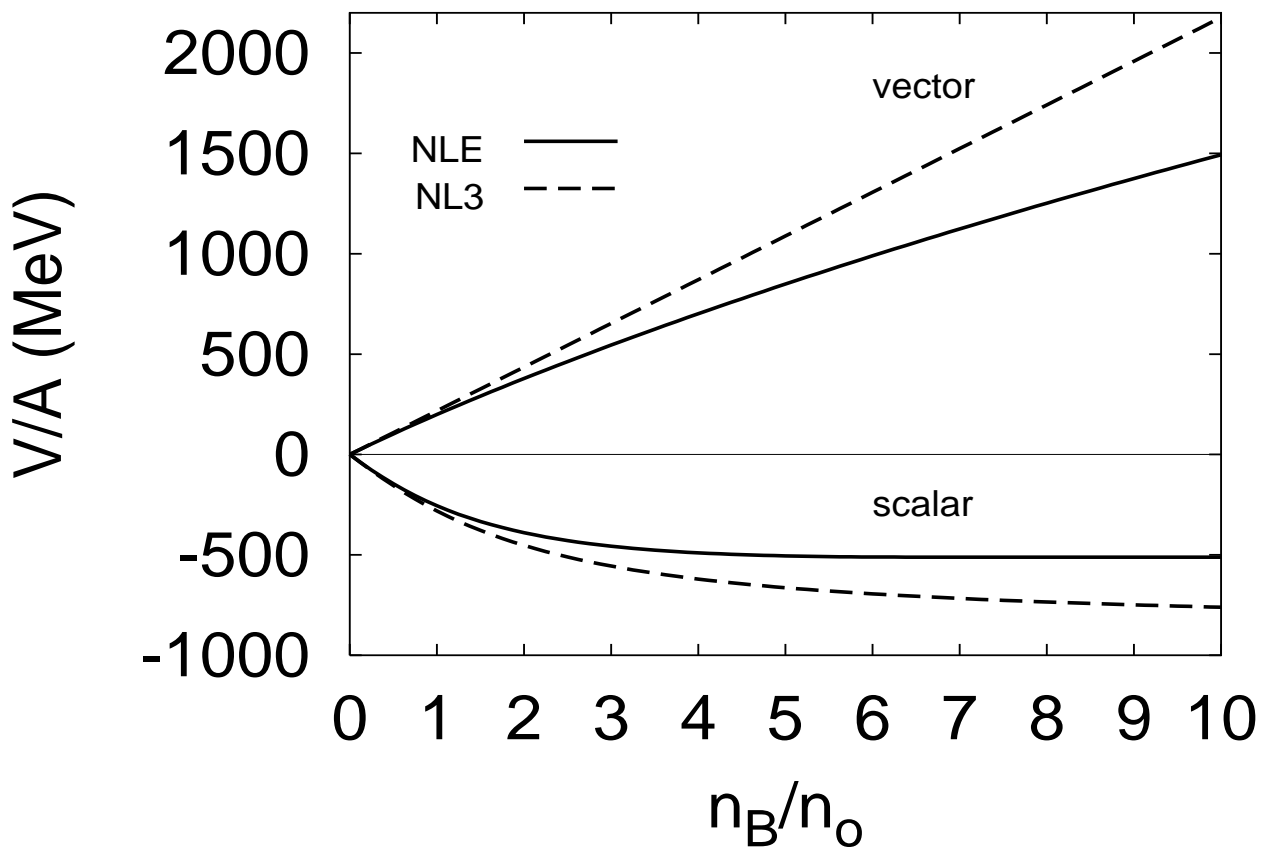


Fig.1 potential energy per nucleon vs baryon density in units of n_0 . The solid lines (NLE) are momentum dependent potentials and the dashed lines (NL3) are without momentum dependent potentials (see the text).

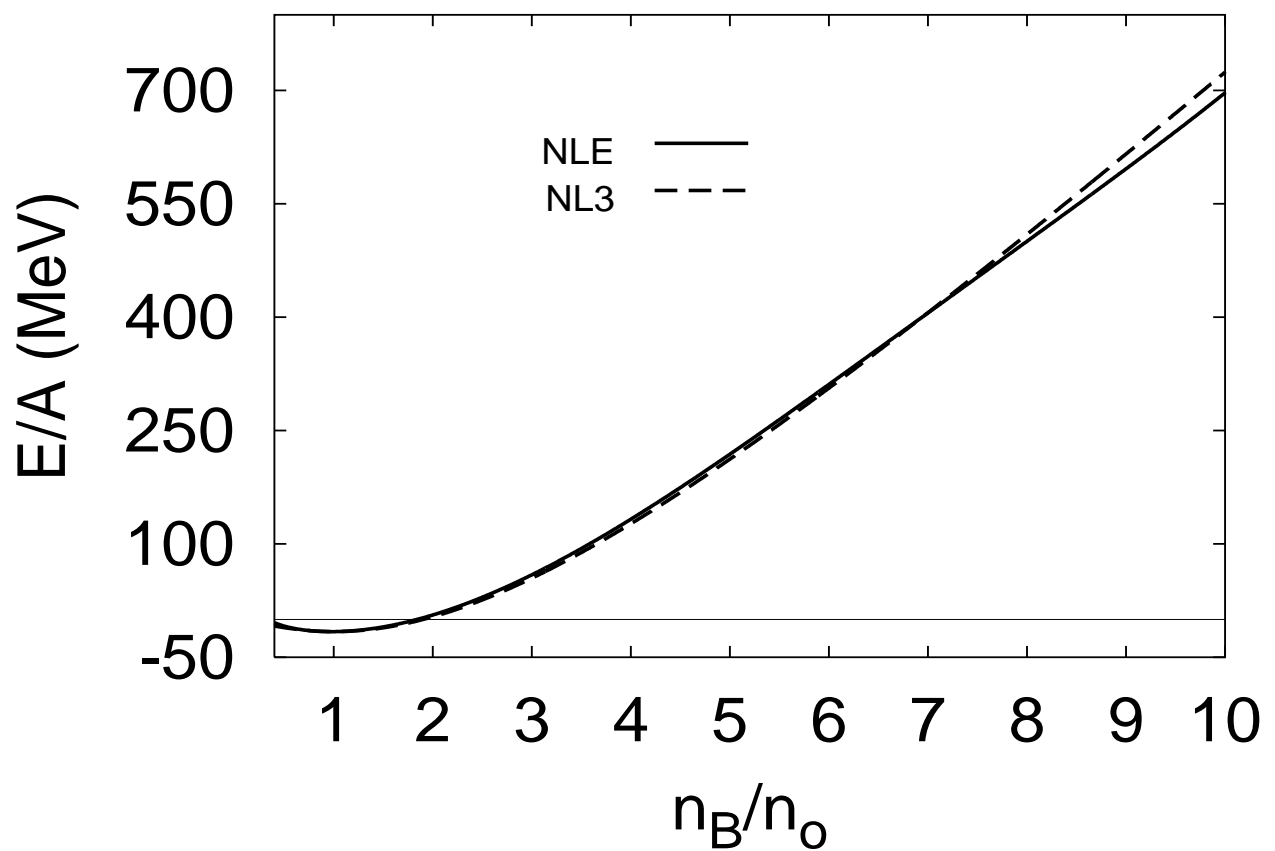


Fig.2 Energy per nucleon vs baryon density in units of n_0 . The models are same as Fig. 1.

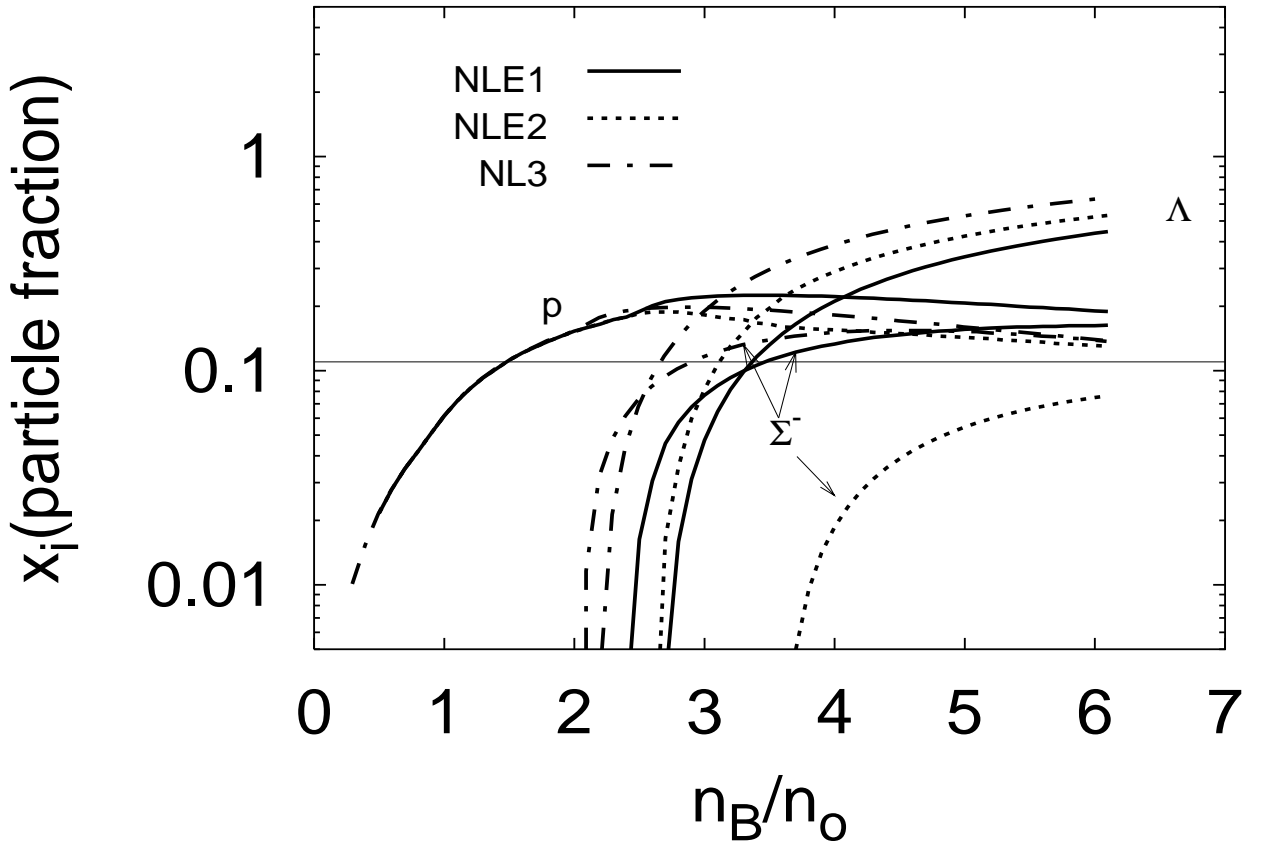


Fig.3 The concentration of each particle ($x_i = n_i/n_B$) vs baryon density in units of n_0 . The momentum dependent potentials have been incorporated in NLE1 (solid line) and NLE2 (dashed line). The dashed-dot lines (NL3) are without momentum dependent potentials. The potential are seen by Λ and Σ are same in NLE1, NL3 (dashed-dot line) and are different in NLE2 (see text).

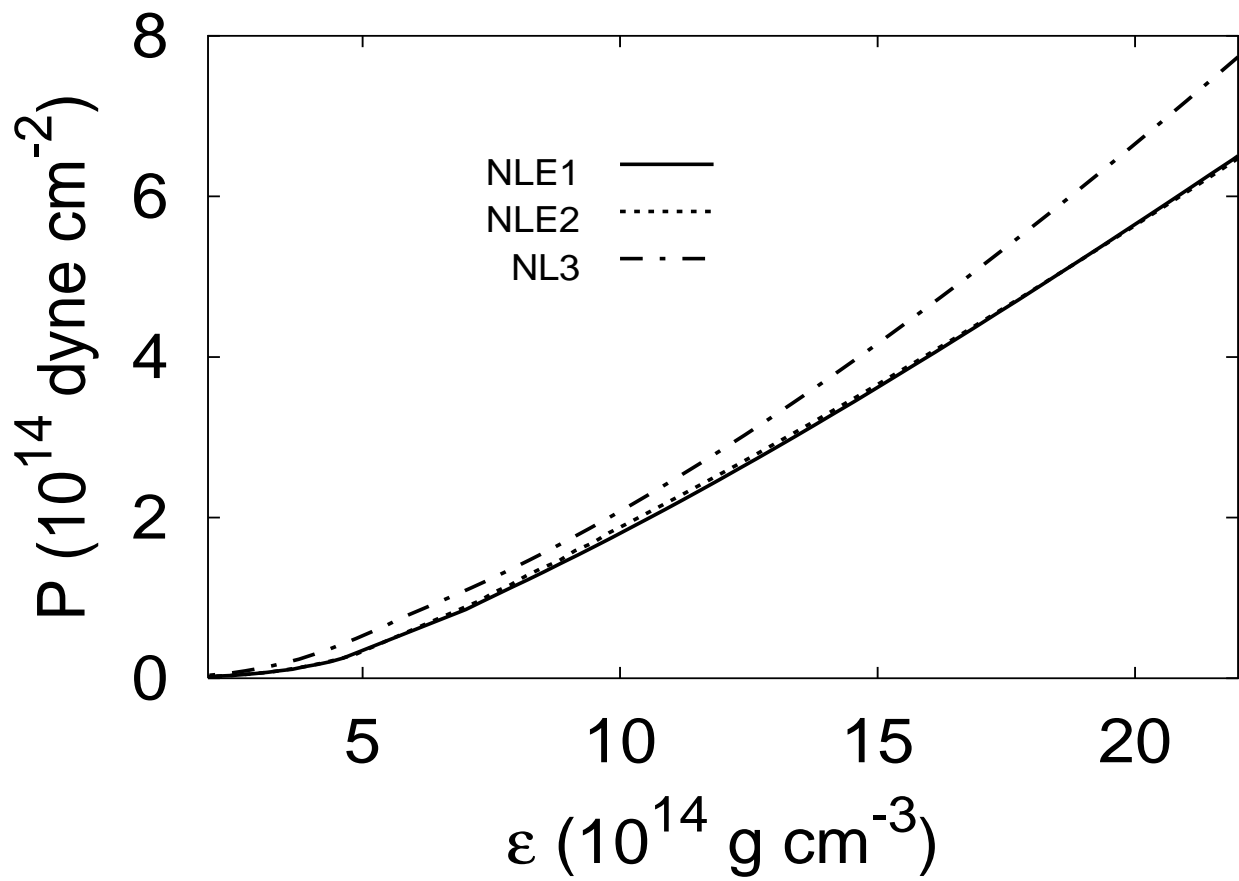


Fig.4 The neutron star matter pressure vs the energy density. The models are same as Fig. 3.

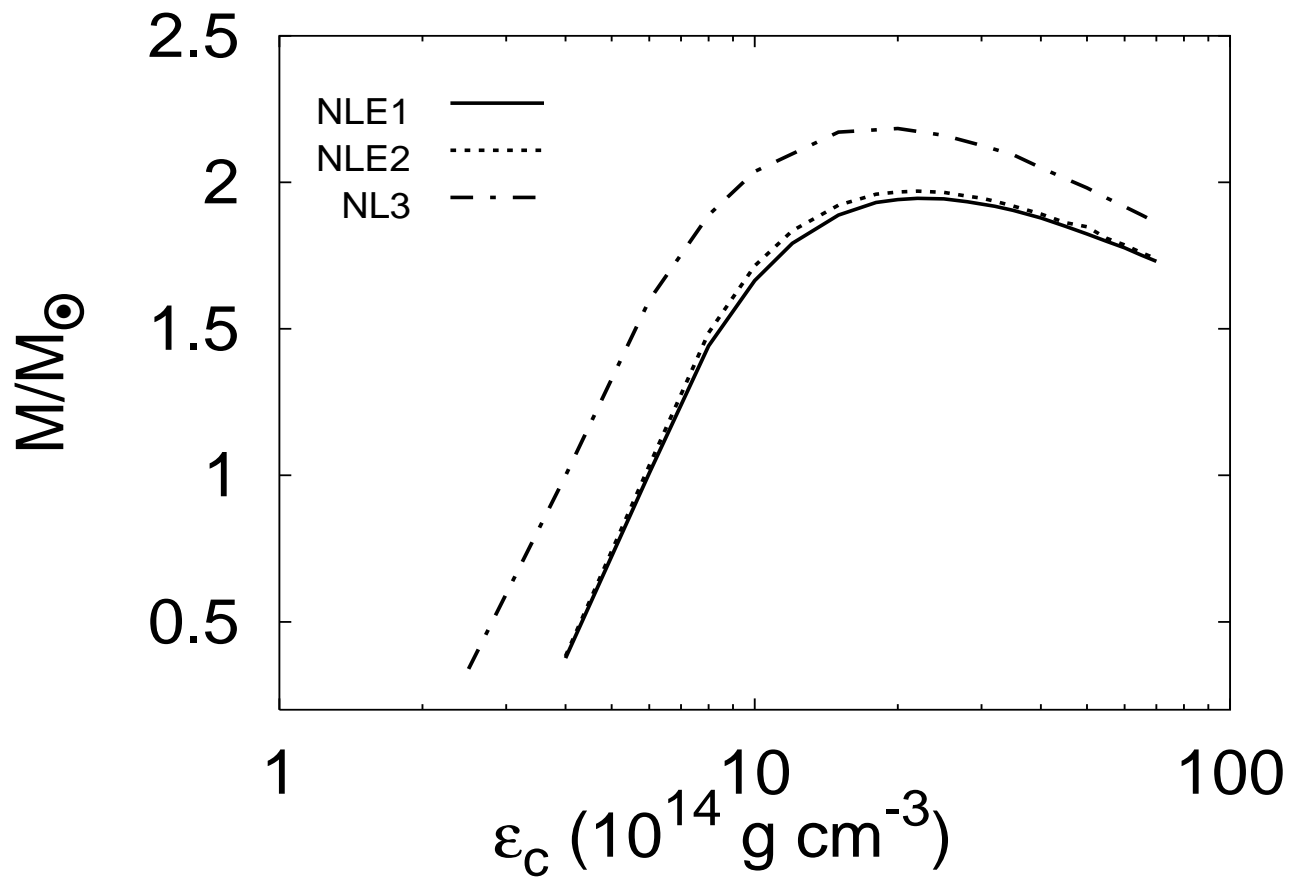


Fig.5 The neutron star mass vs radius. The models are same as Fig. 3.